Persistence and dark current characterization on HgCdTe Short Wave Infrared imagers for astronomy at CEA and Lynred

T Le Goff, N Baier, O Gravrand, O Boulade

Persistence and dark current characterization on HgCdTe Short Wave Infrared imagers for astronomy at CEA and Lynred

T. Le Goff[a], N. Baier[a], O. Gravrand[a], O. Boulade[b]
[a] Univ. Grenoble Alpes, CEA, LETI – 17 Avenue des Martyrs, 38000 Grenoble (France); [b] CEA, IRFU, Astrophysics Department – Orme des Merisiers, 91191 Gif-Sur-Yvette (France).

ABSTRACT

Linked by ESA's Astronomy Large Format Array for the near-infrared ("ALFA-N") technology development program, CEA and Lynred aim at setting up the fabrication of very large IR focal plane arrays (FPA) for astronomy needs. Prior to this project, dark current and image persistence are under investigation for achieving the high level of performance needed by astronomers. During previous characterization of this kind of detector, the FPA appeared particularly sensitive to ROIC electro-luminescence, preventing to observe fainter effects such as persistence. With the mitigation of the glow, the first measurements showed that dark current was dominated by persistence instead of classical diffusion, Auger or Shockley-Read-Hall mechanisms. We propose a dedicated test protocol in order to electrically characterize persistence and an empirical modelling tool to describe it in terms of amplitude and characteristic time constant. The first step consists in removing the residual persistence, allowing to characterize the intrinsic photodiode's dark current, down to 0.03e-/s at 90K on four tested devices. From this reference, the persistence contribution is dramatically minimized and experimental conditions are reproducible, enabling further investigation on persistence to be carried out. Applied on detectors manufactured in the CEA-LETI clean rooms, this protocol aims at a better understanding of the phenomenon. Using an array containing different diode flavours (ie variations in the technological parameters such as diode geometry, passivation…), the characterization scheme described above should bring information about technological contributions on persistence.

Keywords: Persistence, HgCdTe, SWIR imager, astronomy

1. INTRODUCTION

After a bright exposure, short wave infrared (SWIR) imagers for astronomy exhibit an excessive non-linear signal whose time constant is compatible with the integration time used in this application. This phenomenon is called persistence and it limits the performances of the imager and constrains users to operate in degraded conditions. Users solutions to mitigate persistence are either to reduce the operating temperature [1] or to permanently illuminate the detector [2] but it lower the performances of the detector. Post processing data to compensate persistence is possible but requires an unique characterization scheme for each mission such as for the WCF3 camera on the Hubble Space Telescope [3] or the 16 IR detectors from Euclid [4]. Taking into account this phenomenon from the beginning of the manufacturing of these detectors is consequently urgent.

The ALFA project aims at developing large FPA for astronomy in Europe. On phase A project detectors leading to ALFA, classical high performance figures of merit such as low dark current, low noise and high quantum efficiency have already been demonstrated [5]. These test detectors have a different ROIC than on ALFA, the main difference is the nodal capacitance lowered by design on the former detectors [6] and the additional fixed capacitance for ALFA. They however come from the same manufacturing line of the CEA and Lynred clean rooms. We then use these detectors from former projects to characterize persistence and ultimately transfer this knowhow for future ALFA characterization. Since these test detectors are manufactured in CEA-LETI clean room, we have access to all technological parameters and the whole process flow. We will use these information to address the persistence issue with a manufacturer point of view and take into account persistence from design for future detectors developments.

For this purpose we characterize persistence on two detectors: a mono-technology (MONO) one to study the non-uniformities over a single array with a classical technology and a multi pixel geometry (MULTI) array to probe several technological variations in a single measurement. Both detectors are taken from on the same wafer. They are then mounted in a liquid nitrogen cooled cryostat and the output voltage is sampled with an external 4 channels 14 bits data acquisition setup without input adapter that limits the read noise.

The two detector under investigation are 522*648 pixels arrays with 15µm pitch and 2.1µm cutoff wavelength operating at low temperature (100K) with a ROIC architecture based on a Source Follower per Detector (SFD). The ROIC has references pixels surrounding the sensitive 514*640 pixels area. There are also two rows of test pixels including some with a fixed capacitance that can be used as a reference to measure the capacitance of sensitive pixels. The ROIC has 8 video channels and we read the channels 1-4 first then channels 5-8 due to the data acquisition setup. On these tests detectors, the photo-generated carriers are collected in the P/N HgCdTe diode, resulting in a voltage change as the carriers are accumulated in the diode capacitance. The photo generated current is integrated as long as the diode capacitance is not full. This SFD architecture allows to non-destructively read the voltage drop on the pixel several times in order to reduce the read noise and sample an integration ramp in a Up The Ramp (UTR) mode. Collecting data in this UTR mode consumes much memory space and post-processing time but enables to detect any singularity or non-linearity occurring during the integration, notably cosmic ray or persistence.

For its simplicity and compatibility with an in-line characterization, we probe persistence with the electrical stress procedure [7], [8]. It is however not representative to an optical stress or a typical situation encountered by users. For instance it does not allow to probe the influence of the saturation or of the time between the stress and the reset, the so called soak time. Before characterizing persistence, we use the linear dark current as a reference to compare the persistence response for each temperature, also giving access to the activation energy of dark current mechanisms. We then describe qualitatively persistence in terms of amplitude and time constant and analyze their evolution with temperature.

2. DARK CURRENT RESULTS

Prior to characterize persistence, one must be sure that the test environment is under control. Since persistence is dependent on the entire electrical, optical and thermal history of the imager, a simple dark current characterization will reveal if any persistence from previous tests remains. Such reproducibility protocol is demonstrated on our joint paper [12]. We present here further investigation on the temperature dependency of this background linear dark current and the mechanisms involved. This section also introduces the devices under test and the methodology to extract persistence and dark current parameters from the integration ramp. Besides, this analysis of a well-documented astronomical imager parameter is a necessary step towards the interpretation of technological influence on dark current and persistence.

2.1 Extracting parameters of dark current measurements

Figure 1 illustrates a dark current UTR in correlated double sampling (CDS) mode for two pixels of the detector MONO where each point is acquired every 30s for a total integration time of 4h. The high rms noise is due to our data acquisition system, the ROIC noise is negligible in comparison. We distinguish two regimes: a positive or negative initial non-linearity followed by a linear evolution. In order to quantify the non-linearity and extract the dark current per pixel from this UTR we apply the fitting model from Eq.1. It gives the measured output voltage as a function of time including a linear term $\frac{I_{dark}}{C}$ with C the diode capacitance, I_{dark} the dark current of the pixel and an exponential term for the initial non-linearity. The parameter V_1 traduces the amplitude of the non-linearity and τ_1 the time constant. Similar model will be used in the following sections to describe persistence.

$$V_{1\text{explin}}(t) = \frac{I_{dark}}{C} \times t + V_1\left(1 - e^{-\frac{t}{\tau_1}}\right) \quad (1)$$

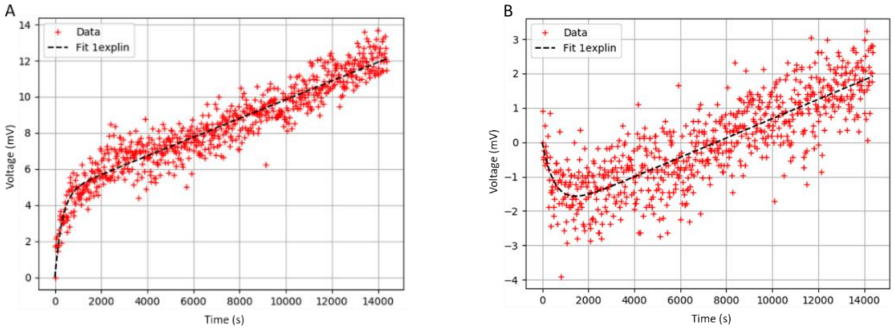

Figure 1. UTR signal of two pixels of detector MONO for a dark current measurement at 100K. The high rms noise that plagues the signal is due to our data acquisition equipment. One can remark that about 4h of integration is necessary to

extract the low dark current of the detector. Fitting parameters are: A. $I_{dark} = 0.06e^{-}/s$, V_1=4.5mV, $\tau_1 = 500s$ and B. $I_{dark} = 0.035e^{-}/s$, V_1= -2mV, $\tau_1 = 310s$.

As the dotted line on Figure 1 shows, the fitting model is robust to extract the dark current after a positive or negative initial non-linearity. The noise on these UTR is dominated by the data acquisition equipment and not by the ROIC noise. The following Figure 2 gives the dark current on all the pixels of detector MONO for the nominal operating temperature 100K and a pixel bias of 400mV. This dark current is homogeneously distributed on the detector, with slightly fewer current and less hot pixels on the right edges.

In order to evaluate the impact of the exponential term of the fitting model on the dark current estimation, we computed the correlation coefficient r between each parameter. A correlation between two parameters would indicate that one parameter compensate the other and therefore their estimation is biased. This checking is repeated for every fitting and we do not report any correlation coefficient above 0.5, the limit value to consider that there is a correlation between two parameters.

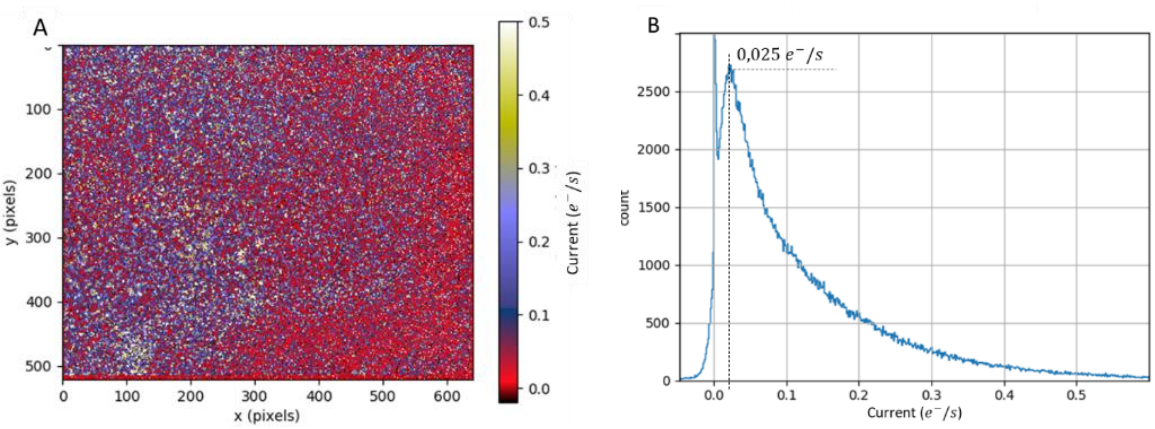

Figure 2. Dark current mapping and histogram of detector MONO for an operating temperature of 100K. The median dark current is $0.025\ e^{-}/s/pix$, the distribution tail corresponds to hot pixel and the $0\ e^{-}/s/pix$ peak is due to unfitted pixels. They represent less than 5% of the total pixels.

Besides, the initial non-linearity has a small amplitude and a short time constant for most pixels. The noise of the data acquisition system is on the order of 500µV, much higher than the combined ROIC noise and dark current shot noise. It consequently forces us to extend the acquisition time to extract the dark current and can be misinterpreted by the exponential fit as a small initial non-linearity. The time constant and amplitude distributions of the initial non-linearity do not change with temperature from 110K to 85. Above 110K the non-linearity is negligible compared to the dark current and data acquisition read noise, consequently the fitting model fails to fit the data. Therefore, a simple linear fit is more appropriate for temperatures higher than 110K.

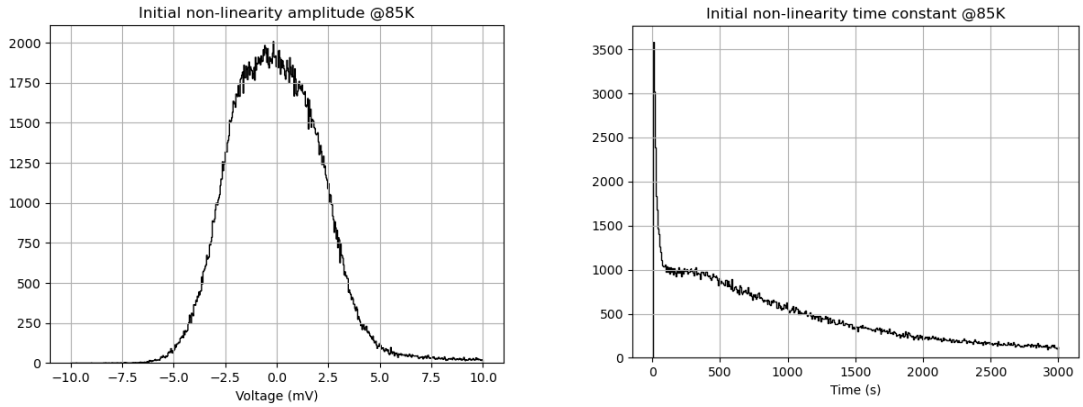

Figure 3. Initial non-linearity amplitude and time constant histograms at the operating temperatures 85K.

Now this initial non-linearity is considered, let's take a closer look at the dark current behavior in temperature and the mechanisms involved.

2.2 Activation energies of dark current mechanisms

We repeated this procedure to extract dark current, ie a linear fit for temperatures in the range from 165K to 115K and a fit with model Eq.1 for measurement at 110K and below. Figure 4 synthesizes the evolution of the median dark current in a log plot as a function of 1/T. Two behaviors then appear: a fast decrease at high temperature followed with a moderate one and a transition around 115K. The dark current model presented on Eq.2 includes two activation energies in order to fit the two mechanisms involved in dark current. The fit of the 17 points of Figure 4 with the logarithm of Eq.2 gives activation energies $E_{a1} = 0.35eV$ and $E_{a2} = 0.08eV$.

$$I_{dark}(T) = J_{01}e^{-\frac{E_{a1}}{T}} + J_{02}e^{-\frac{E_{a2}}{T}} \quad (2)$$

The gap energy of this detector is about 0.6eV, thus E_{a1} is close to mid gap and should correspond to generation-recombination current in the depletion region of the diodes. The smaller energy of E_{a2} should correspond to a family of trap in the depletion region or surface traps. Energies activation of defects in HgCdTe compounds in the SWIR range are unfortunately not well documented. Besides, as the band gap of this material changes with the cadmium fraction, the energy of traps changes too and it is hazardous to extrapolate trap energies of long or mid wave range material to SWIR[9].

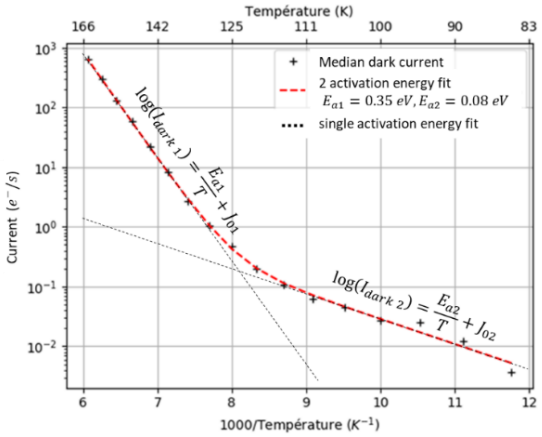

Figure 4. Log plot of the median dark current versus 1/T. The dotted lines represents the activation energies of two mechanism involved in dark current.

Applying the same fitting model on a pixel level reveals that all pixels have similar energies activation as the histogram from Figure 5 shows. The distributions peak at slightly different energies than with the median fit, giving $E_{a1} = 0.32eV$ and $E_{a2} = 0.06eV$. The Local maximum of E_{a2} centred at 0.35eV is due to pixels whose dark current could not be estimated at low temperature due to the initial negative non linearity.

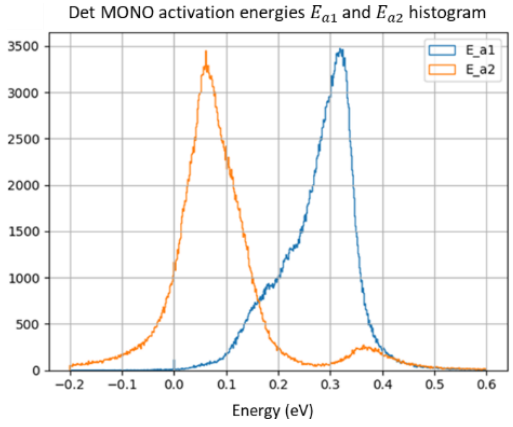

Figure 5. Pixel level energies activation histogram. The distributions of E_{a1} and E_{a2} are plotted on the same graph.

Mappings of activation energies on Figure 6 shows that the distributions are not spatially homogeneous. Edge effect strikes pixels on the right side of the detector, they have higher activation energy E_{a1} and smaller E_{a2}. These pixels also tends to have mostly negative initial non-linearity.

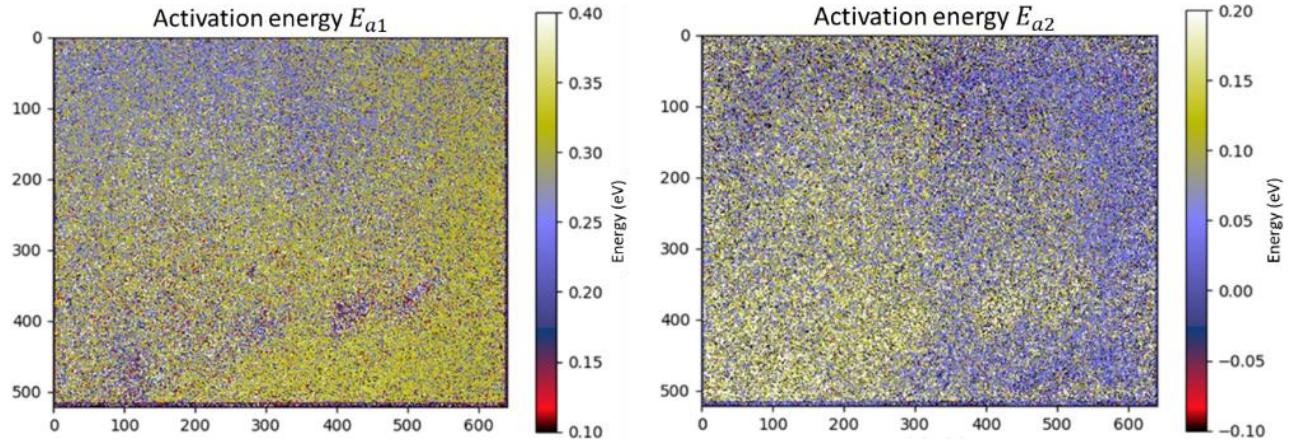

Figure 6. Activation energy mappings of E_{a1} and E_{a2} on detector MONO.

To sum up, the classical technology of detector MONO demonstrates generation current from the depletion region in the temperature range from 165K to 120K. Below 110K a mechanism with a low activation energy $E_{a2} = 0.06\ eV$ limits the dark current decrease. Even so, we report dark current as low as $0.025e^{-}/s$ at the nominal operating temperature, 100K. If all the pixels have similar activation energies, they are not uniformly distributed on the detector. Pixels on the right side present higher E_{a1}, smaller E_{a2} and negative initial non linearity. These non-uniformities of the classical technology must be taken into account before interpreting the results of the detector MULTI.

2.3 Technological influences on dark current with detector MULTI

With detector MULTI, we investigated the influence of geometrical parameters on dark current and persistence. Two different metallisation sizes ϕ_{met} A and B and three P doped region sizes ϕ_{imp} 1, 2, 3 allows to probe the influence of a bulk dominated or surface dominated pixel behavior. Figure 7 illustrates the two parameters involved with ϕ_{met} A < ϕ_{met} B and ϕ_{imp} 1 < ϕ_{imp} 2 < ϕ_{imp} 3. With ϕ_{met} A the bulk behavior dominates, with ϕ_{met} B the surface behavior dominates.

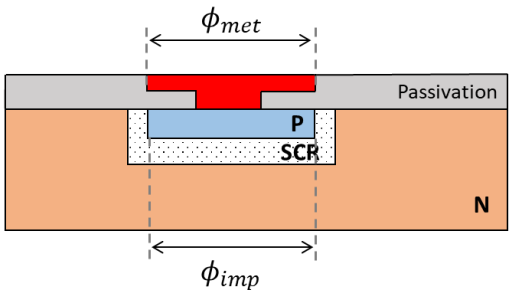

Figure 7. Minimalist diagram of a pixel. From top to bottom are represented the metallization for the P implanted region contact with diameter $\boldsymbol{\phi_{met}}$, the passivation of the surface, the P side of the diode with diameter $\boldsymbol{\phi_{imp}}$, the space charged region and the N type HgCdTe absorbing material.

Dark current as a function of temperature is obtained with the same protocol as with detector MONO, taking into account the different diode capacitances of each technology. This parameter is obtained with the reset noise method on test pixels without diode and a known input capacitance as reference. The evolution of the diode capacitance for each technology as a function of the applied voltage is presented on Figure 8. Technologies with metallization B do not show any capacitance dependency with the implantation size and diode voltage. Conversely, technologies with met A presents a capacitance dependency expected for a diode, with higher capacitance as the applied voltage decreases and implantation size increases. Technologies with the larger metallization have a capacitance that does not follow a diode capacitance behavior. Their constant capacitance would be more related to the metal-insulator-semiconductor (MIS) structure formed at the interface

between the absorbing $H_g C_d T_e$ bulk and the passivation. Indeed this kind of structure present a constant capacitance if they stay in an accumulation regime, where there is not depletion in the semiconductor at the interface.

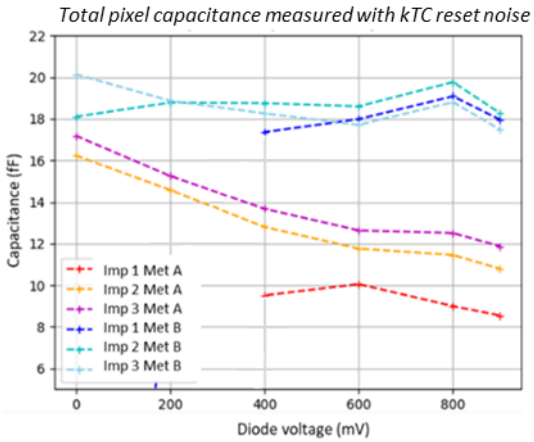

Figure 8. Mean diode capacitance of each technology of detector MULTI plotted as a function of the reverse diode voltage.

Since diode capacitance has a direct impact on the estimation of the dark current we use the estimated capacitance values at 400mV, the same applied voltage than for dark current measurement. Figure 9 represents the dark current at 100K, with the table and the dotted lines on the left of the figure delimiting 12 sets of 44 rows, each set representing a technology variation. Cosmetic variations on the dark current mapping can be attributed to whether the metallization is A or B. For metallization A, the implantation diameter appears to have little impact on the cosmetic since there is much spatial dark current variation within a single technology. They also exhibit a very long negative initial non-linearity at temperatures below 115K, preventing to extract the dark current and causes the negative values on the mapping. Technologies with metallization B are more robust to spatial variation and different behaviors depending on the implantation diameter can be observed. Technology MET B IMP 1 is the smoothest, with few hot pixels and little spatial variation. The line noise on the second set of rows of techno MET B IMP 1 is an artefact from the data acquisition system. Dark current of techno MET B IMP 2 is unusable at temperatures higher than 90K due to a large number of hot pixels and strong pixel cross-talk. Technology MET B IMP 3 is similar to MET B IMP 1 but has more hot pixels.

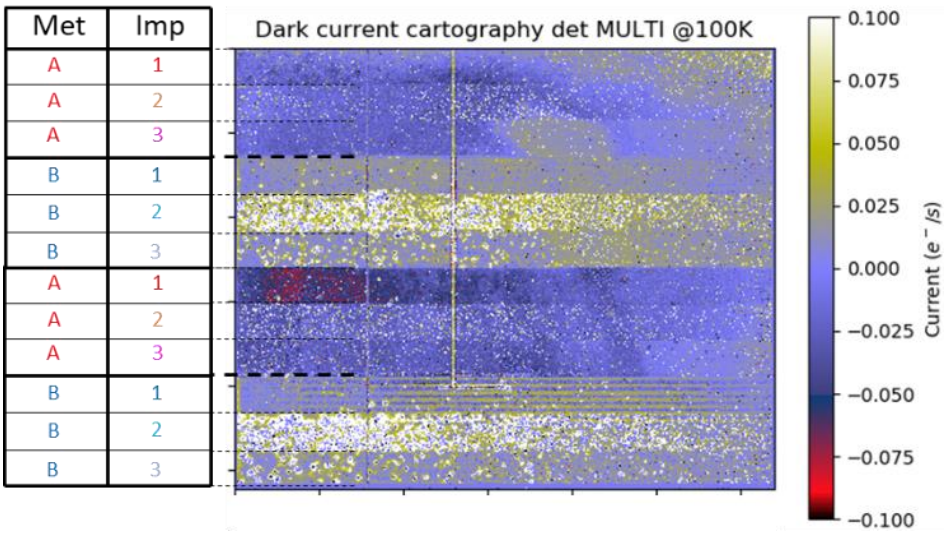

Figure 9. Dark current mapping of det MULTI at 100K with corresponding technology of each set of rows.

The median dark current of each technology and detector MONO is reported as a function of temperature on Figure 10. Apart from the negative dark current below 115K of technologies A1 and A2, all technologies including the standard one

from detector MONO presents the same behavior in a median value. There is no difference between technologies with MET B and detector MONO on the low temperature range, enhancing the stability of this technology.

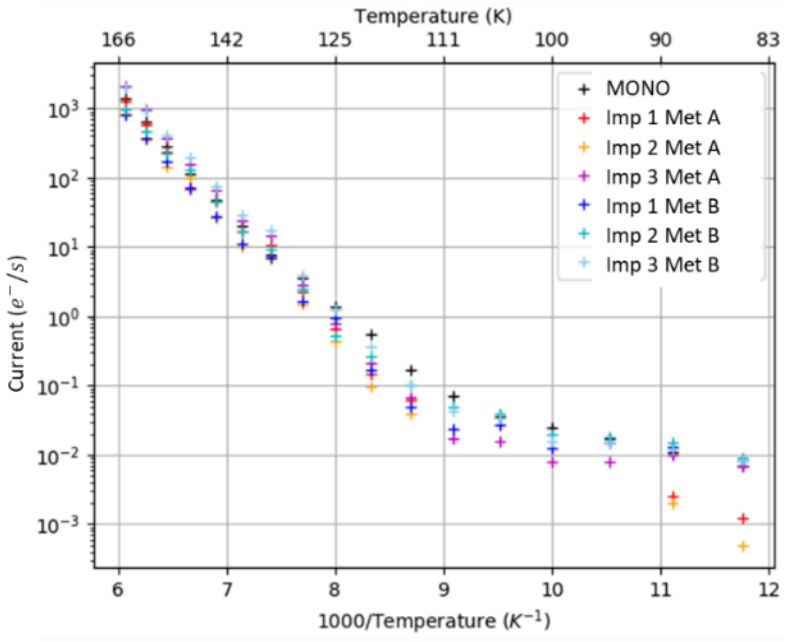

Figure 10. Dark current dependency on temperature of each technology and detector MONO.

Some differences appears with pixel level activation energies. E_{a1} has a value close to the mid-gap, it represents the generation current mechanism in the temperature range from 165K to 115K. Technologies MONO and the ones with the large metallization size have activation energies that do not depends on the implantation size. However technology MET B IMP 2 is dominated by hot pixel mechanisms, its activation energy distributions are much dispersed. Pixels with the small metallization size sees their activation energy E_{a1} increasing with the implantation size. They yet have too many pixels with negative dark current at low temperature to fit an accurate activation energy E_{a2}. With such low currents, the measurement equipment is pushed to its limits thus the very low dark current of technologies A is often fitted as a negative one because of the poor signal to noise ratio.

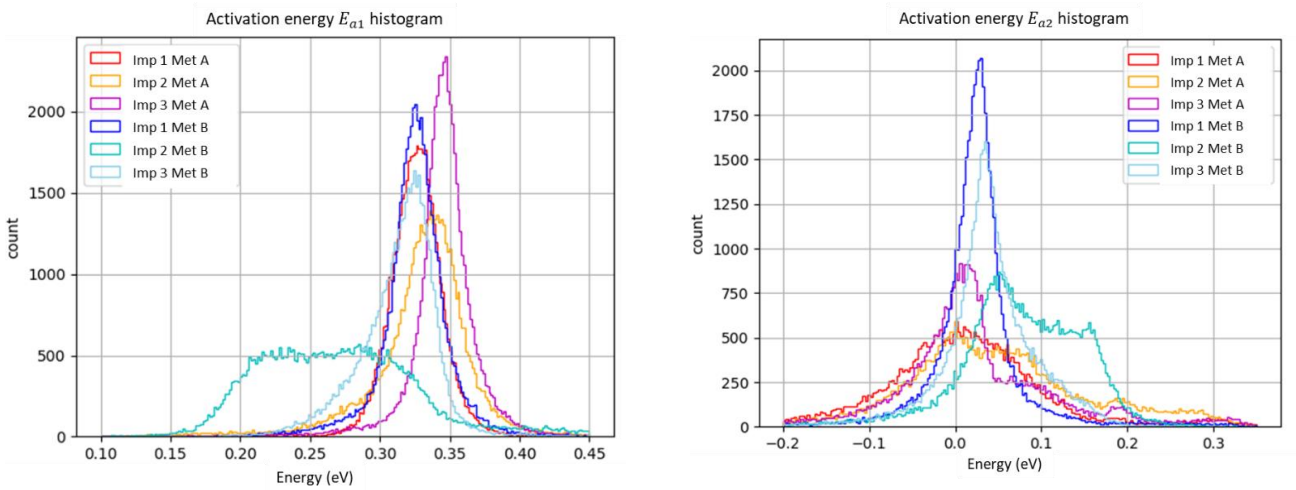

Figure 11. Pixel level activation energies histograms at high and low temperature E_{a1} and E_{a2} of each technology.

Metallization diameter has a major impact on dark current behavior in temperature. Detector MONO shows some non-homogeneities on its edges, they are smoothed with metallization MET B while MET A spreads them. The initial non-

linearity has fewer impact on MET B, this might be due to a lower dark current with MET A. The implantation size does not have an impact on dark current for techno A and only changes the number of hot pixels for techno B.

Dark current characterization was a necessary step as it represents the minimum background signal of the detectors on which persistence will be added. It also revealed the major impact of the metallization size and that techno A is subject to an initial negative non-linearity. Now, persistence will allow to probe different properties of the pixel, revealing other influences of the diode geometry.

3. PERSISTENCE DEPENDENCY ON TEMPERATURE AND DIODE GEOMETRY.

The classical dark current characterization already revealed diode geometry influences on the pixel behavior. Now, characterizing persistence on a multi technology detector is twofold: it allows to search for a technology that mitigates persistence and is a powerful tool to finely probe the impact of a given technological parameter. Indeed, persistence characterization interpretation can be linked to the Deep Level Transient Spectroscopy (DLTS [10]) technique but on a complex device. Therefore, persistence can be used as a complementary tool in a characterization scheme on a process line to probe subtle impact of a technological parameter.

3.1 Principle of the measurement

Persistence characterization is performed with the electrical stress procedure for its simple setting up and easier interpretation than photonic stress [7]. Its principle can be divided in three steps:

- Setting the pixel on an equilibrium state such as when performing a dark current measurement.
- Suddenly changing the applied voltage on the pixel to force it out of the equilibrium state.
- Following the pixel signal as it responds to the electrical excitation.

This protocol is not representative of an optical stress persistence characterization or of a typical astronomical observation. Indeed the objective here is not to calibrate persistence on a detector but to study technology and temperature impact on this phenomenon. Consequently this protocol only has two parameters, the temperature and the amplitude of the electrical stress. The soak time usually investigated when characterizing persistence is with this protocol set to infinity when performing the equilibrium state. Persistence characterized with this protocol is consequently a worst case scenario for astronomy application but maximises the persistence signal. Indeed in this case all traps in the SCR or at the interface are occupied and all trapped mobile charges in the passivation are at their equilibrium position. All these defects will respond to the quick voltage change and consequently induce a large persistence response.

The reproducibility of the equilibrium state is essential and the impulse response of the pixel must be orders of magnitude higher than the dark current background to be properly interpreted. We propose to qualitatively analyse persistence amplitude and time constant as a response of an impulse stress from 0V bias to 600mV reverse bias as function of temperature. The fitting model to extract these parameters is similar to the one used to measure dark current, Eq.3 and Eq.4 gives the output signal of a pixel as a function of time.

$$V_{3\exp}(t) = V_1(1 - e^{-\frac{t}{\tau_1}}) + V_2(1 - e^{-\frac{t}{\tau_2}}) + V_3(1 - e^{-\frac{t}{\tau_3}}) \quad (3)$$

$$V_{3\,\exp lin}(t) = \frac{I_{dark}}{C} \times t + V_1(1 - e^{-\frac{t}{\tau_1}}) + V_2(1 - e^{-\frac{t}{\tau_2}}) + V_3(1 - e^{-\frac{t}{\tau_3}}) \quad (4)$$

The linear term on Eq.4 traduces that for some pixels the dark current can dominate persistence current for long integration times or at high temperature. We fit the data of each measurement with the two models and then select the one that is the most appropriated to attribute persistence amplitudes and time constants. The two models includes three exponentials not for physical reasons but because persistence spreads over several orders of magnitude of time. Therefore each exponential term fits one order of magnitude of time, they are not related to any charge trapping/emission process. This non physical fit only aims at giving quantitative values to persistence and compares these values between technologies and temperatures. Increasing the number of exponentials does not improve the fitting quality, it only fits shorter time constants. Figure 12 shows the several steps of the fitting process, giving a total persistence amplitude $V_{tot} = V_1 + V_2 + V_3 = 190mV$, time constants $\tau_1 = 30s$, $\tau_2 = 430s$, $\tau_3 = 2200s$ and a dark current $I_{dark} = 0.045e^-/s$. Even if each amplitude or time

constant term reveals a different persistence mapping, the total amplitude is of most interest to analyze persistence as a function of temperature.

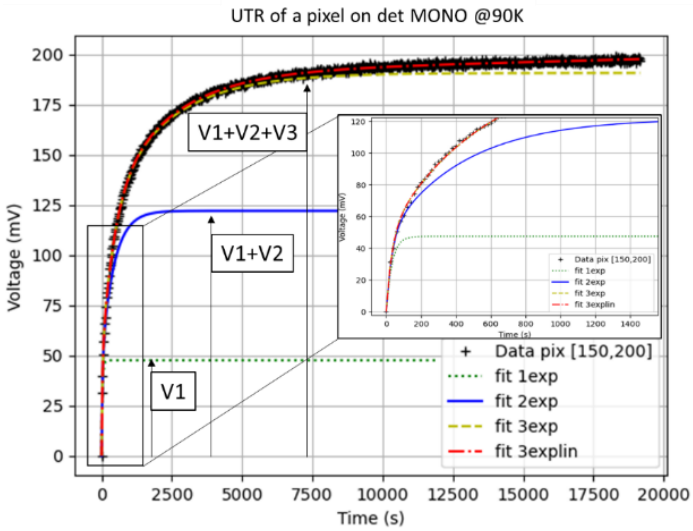

Figure 12. UTR of a pixel from detector MONO at 90K and the several steps of the fitting. The first exponential fits the very first seconds of the UTR, the second one fits the first hundreds of seconds and the last exponential fits the longer time constant. The linear term of the 3explin model finally fits the dark current when persistance current is negligible.

Please note that we plot the persistence response in volt unit instead of an equivalent charge in e^- unit. Indeed the measured signal of a pixel is its voltage change over time. However this voltage change can be due to an accumulation of charge in the pixel thus directly giving a current or can be the result of a capacitance variation and therefore a conversion gain variation. The diode capacitance is a function of the applied voltage and of the fixed charge in the space charged region:

$$C_{\text{diode}} = A\epsilon\sqrt{\frac{qN_{SCR}}{2\epsilon V_{diode}}} \tag{5}$$

With A the surface of the diode, ϵ the permittivity of the $H_g C_d T_e$, V_{diode} the diode voltage and N_{SCR} the fixed charge in the space charged region (SCR). During the equilibrium state the only fixed charges are the dopant $N_{SCR} = N_D$. When the diode is electrically stressed, charged traps n_T are revealed and their charge contributes to the capacitance of the pixel since $N_{SCR} = N_D - n_T(t)$. Consequently the voltage of the pixel changes both due to the emission of carriers from the traps and to the capacitance change resulting from charge change of the traps n_T when they emit their carrier. The DLTS analysis uses this phenomenon to detect trap families of semiconductor devices [10] and a similar process occurs during a persistence characterization. However no trap family can be extracted from persistence measurement as a function of temperature because the structure of a pixel is much more complex than a DLTS test structure, mixing multiple contribution from the bulk, the surface etc…

Unlike the capacitance as a function of the applied voltage calibration, the trap density and its temporal dynamics in the SCR is unknown. It is besides not possible to neglect the trap density compared to the doping density since the residual doping, ie the uncontrolled doping of the material, is usually only ten times smaller than the controlled doping N_D. A charge change in the SCR N_{SRC} of 10% will result in a capacitance change of 5% and therefore impact the persistence signal. Moreover, the total pixel capacitance is not only related to the diode capacitance, it is just the only contribution with limited unknown parameters.

Since in a SFD pixel we measure a voltage change across the P/N diode, the voltage change induced by persistence is due to a charge accumulation and a gain variation. For a classical dark current or incident flux measurement, the only influence on capacitance variation is the voltage change on the pixel due to the slow charge accumulation. The conversion gain can be considered constant over a large voltage range. However when persistence is involved the pixel suddenly step out of its equilibrium state. The applied voltage changes and the charge density in the SCR in largely compensated by the negative charge of occupied traps. Consequently mechanisms involved in both charge emission and pixel capacitance variation must be taken into account to model persistence.

The above consideration on the influence of capacitance variation on persistence must be taken into account to also compare persistence response on technologies whose capacitance is not the same.

3.2 Persistence uniformity and temperature dependency with detector MONO

Performed for temperatures from 130K to 85K, persistence measurement and associated pixel level fits give the total persistence amplitude histograms as a function of temperature on Figure 13. The total amplitude shifts from 160mV at 130K to a constant value of 180mV from 100K and below. This amplitude is equivalent to 30% of the stress amplitude. This amplitude increase can be attributed to a coupling between the exponentials and the linear term of the fitting, minimizing the persistence at high temperature when the dark current is still high. At lower temperature the persistence amplitude is more accurately estimated since the dark current stays negligible before persistence until there is barely no more persistence. Consequently the number of defects revealed do not change with temperature but the relaxation changes. The mapping on Figure 13 presents the best fit of the total persistence amplitude. While the center and the lower right side of the detector is homogeneous, the edges on the half right exhibit a grainy structure with amplitudes about two times lower than on the center and a longer time constant.

If the origin of this non uniformity and the mechanisms involved are not yet clear, such behavior was never recorded before neither in the literature nor on detectors from CEA clean rooms. It points out the relevance of persistence characterization as a powerful tool in a detector process line to observe second order manufacturing parameter fluctuation.

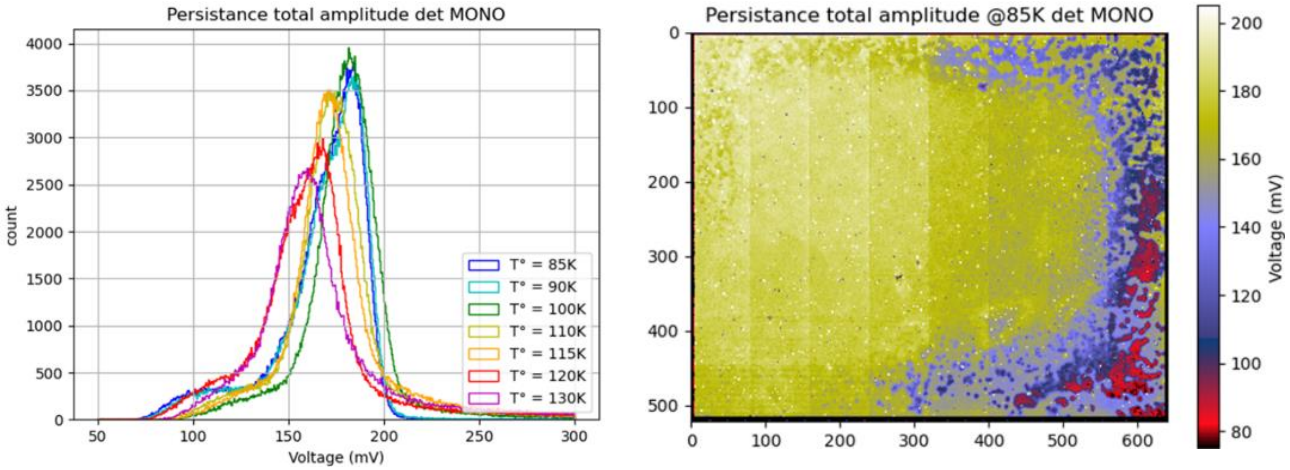

Figure 13. Total persistence amplitude histograms plotted for several temperatures and its mapping at 85K.

The persistence amplitude does not decrease at lower temperature, it even seems to stay constant over a large temperature range. The capture/emission process of traps is expected to freeze below a given temperature but cannot be reached with our liquid nitrogen cooled cryostat.

Unlike the total amplitude, persistence time constant largely varies with temperature. The first time constant namely τ_1 of the models is of limited interest since it is shorter than the sampling time of the UTR. The evolution of medium and long time constants τ_2 and τ_3 with temperature is plotted on Figure 14. For temperatures of 110K and 100K the time constant τ_2 is misestimated by the fit. At the nominal operating temperature, persistence decays with $\tau_2 = 500s$ and $\tau_3 = 3000s$ on average with non-uniformities similar to the total amplitude mapping. Consequently 70% of the persistence decays within the first ten minutes but it takes hours for the persistence current to be negligible compared to the linear dark current. Continuing to cool down the detector could lead to time constants longer than the typical integration time used in astronomy but persistence will remain.

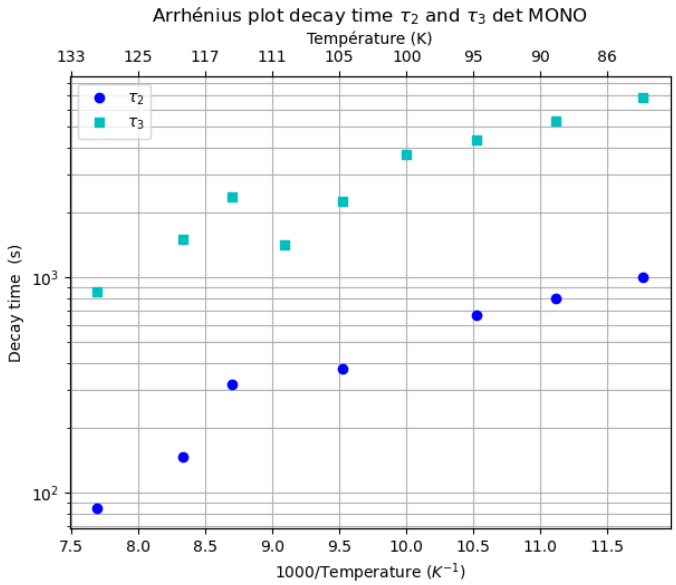

Figure 14. Arrhénius plot of persistence time constant evolution with temperature.

The usual analysis of the time constant as a function of temperature is to produce an Arrhenius plot, ie to plot the logarithm of τ as a function of $1/T$ with T the temperature to extract the activation energy of the trap family involved on the emission process. Such plot cannot lead to this analysis in the case of persistence analysis since the fit used to extract the time constant is only qualitative, not based on physical signification. Besides, multiple trap families could be involved on persistence, including trap continuum in the bulk, in the passivation or at the interface between the bulk and the passivation layer thus misleading the global time constant estimation. Therefore even if the persistence time constant appears to have a linear evolution on the Arrhénius plot it only gives the trend on which persistence gets longer when temperature decreases. On a Mid Wave Infra Red detector H2RG from Teledyne, S. Tulloch presented an increasing persistence amplitude when temperature increases between 41K and 55K [11]. We would obtain the same result using a constant integration time like in this reference.

In the same way as for dark current, the detector MONO is the reference point to compare technological impact on detector MULTI and to interpret the non-uniformities. Persistence on the reference detector has a constant amplitude with temperature about 30% of the amplitude stress and long time constant on the order of 3000s at 100K. Non-uniformities take the form of a grainy structure on the right edges and the center is quite uniform.

3.3 Technological influence on persistence

The same persistence protocol is applied on detector MULTI, the 0V to 600mV electrical stress is repeated on the temperature range from 120K to 85K. Figure 15 compares the total amplitude of each technology on detector MULTI at 100K.

The cumulative histogram emphasizes the difference of total amplitude between the technologies with MET B and MET A, the first having 50% lower persistence amplitude and more homogeneity. The mapping reveals that there are two populations on technologies with MET B due to an inhomogeneity on the center right of the detector. Unlike on detector MONO, the abrupt grainy structure is not present, instead the non-uniformities spread on a larger scale on detector MULTI. The metallisation size can explain both the difference in homogeneity and amplitude between technologies with MET A and MET B. Capacitance measurement from Figure 8 indicated that the capacitive behavior is dominated by the MIS structure at the surface for the larger metallization. In other words the capacitance variations of the diode structure has a negligible influence with regard to the constant MIS capacitance. Moreover, the conversion gain of technologies with MET B is smaller than MET A, resulting in a smaller voltage change for the same charge accumulation. Persistence on technologies with MET B appears to be less impacted by persistence due to their smaller conversion gain. Non uniformities are also smoothed by the larger capacitance of technologies with MET B, they are up to 30% with MET B and on the order of 50% with MET A.

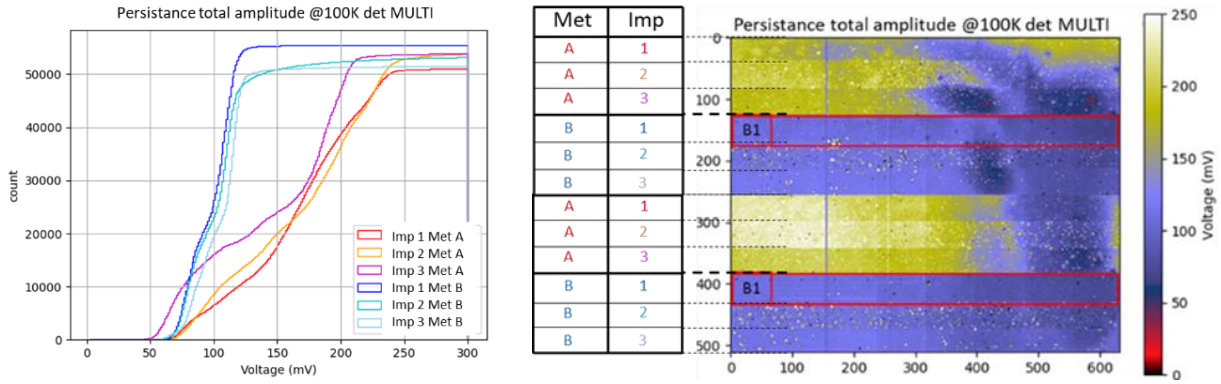

Figure 15. Persistence total amplitude histogram at 100K of each technology and their spatial distribution on a mapping. A focus will be made on technology MET B IMP 1, therefore it is pointed out by red boxes on the mapping.

The influence of the implantation size is a bit more subtle to interpret due to its weak impact and the large non uniformities. With larger implantation size the space charge region increases, thus if the only mechanism involved in persistence is the amount of carriers emitted from traps from the SCR, the persistence amplitude should increase the same way. This behavior is indeed present for technologies with large metallization. On MET A technologies the order of the persistence amplitude increase is inverted. The largest implantation size has the smallest persistence. This inconsistency can be solved taking into account the capacitance of each technology. Since the technology with the larger implantation size also has the larger capacitance, its conversion gain is smaller. As a consequence persistence has fewer impact on this technology than the others with smaller implantation size when plotted in voltage unit. Still, the non-uniformities of this technology mitigates this interpretation and the impact of the implantation size is weak.

With lower persistence amplitude, the technology with larger metallization recovers faster after the electrical stress as well. The long time constant τ_3 is plotted on Figure 16 at the nominal operating temperature 100K for all the technologies of detector MULTI. When technologies with the small MET A have a time constant on order or longer than the total integration time of four hours, the persistence current on pixels with larger metallization becomes negligible compared to the dark current in 2500s, i.e. four times shorter. This wide difference can also be the consequence of a negligible dark current on small metallization technologies. The persistence is apparently longer on MET A since there is no linear dark current. Technologies with the larger metallization size show less persistence because they have a smaller conversion gain and fewer capacitance change with diode voltage at least. The larger metallization also changes the mechanical stress applied on the passivation and the surface. Since the $H_g C_d T_e$ is a piezoelectric material, the electrical environment of traps in these regions of the pixel changes, influencing their properties and then leading to a different persistence time decay.

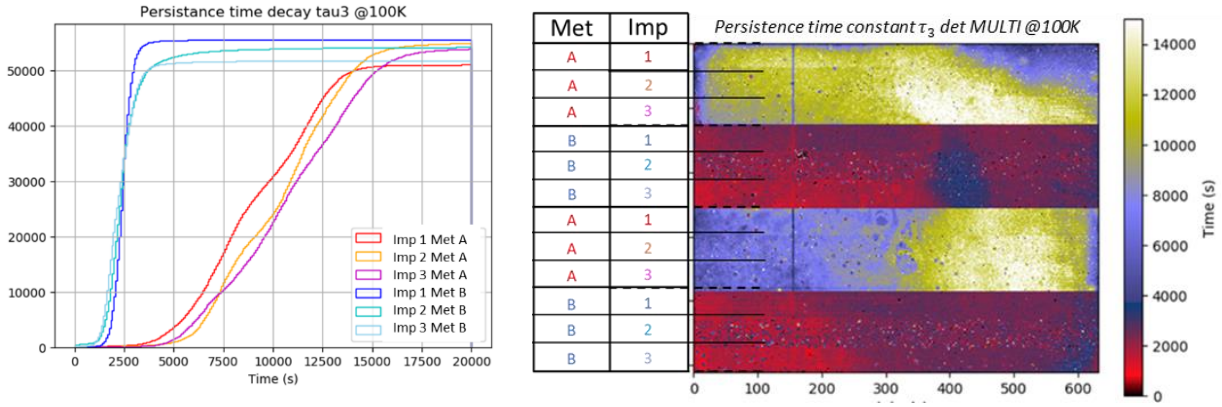

Figure 16. Persistence time constant cumulative histogram at 100K of each technology on detector MULTI and their spatial distribution on a mapping.

At a constant temperature, the metallization has a major impact on both persistence amplitude and time constant.

3.4 Influence of the temperature

Persistence evolution with temperature is not as straightforward as on detector MONO. Large non uniformities on technologies with MET A give broad amplitude and time constant histograms, resulting in an unclear behavior of this technology with temperature. The same goes for total amplitude on technologies with larger metallization, this parameter is still under investigation. Nevertheless, time constant on technology MET B IMP 1 is uniform and presents a similar evolution on temperature than detector MONO. Figure 17 presents an Arrhénius plot of time constants τ_2 and τ_3, a bit shorter than on detector MONO but with the same trend on temperature.

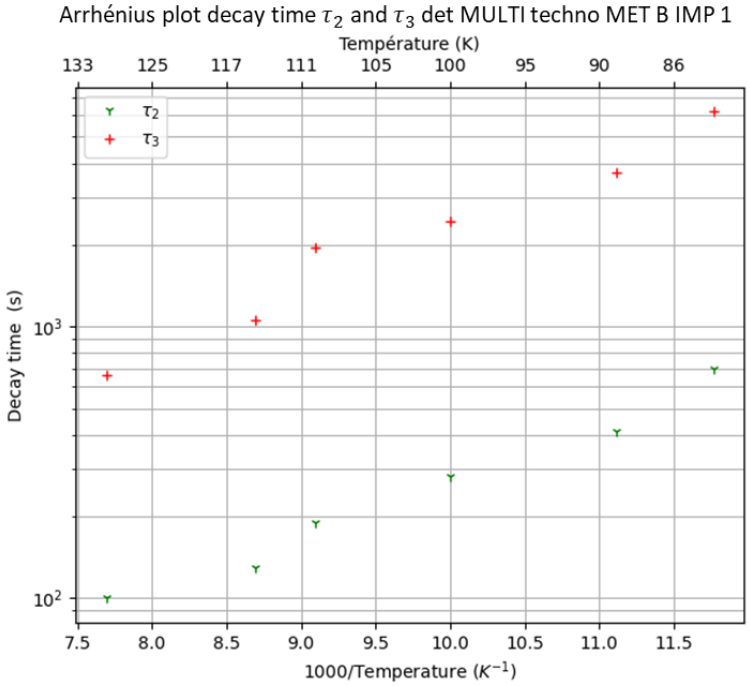

Figure 17. Arrhénius plot of time constants τ_2 and τ_3 on technology MET B IMP 1 from detector MULTI.

For all technologies characterized, persistence has a similar evolution with small total amplitude changes and a longer time constant as temperature decreases. Mechanisms involved in persistence do not freeze in the temperature range investigated since the total amplitude does not dramatically drops. Nevertheless reducing the temperature will indeed extend its time constant until making it much longer than the minute integration time range used in astronomy. The geometry of the pixel has a great impact on both the amplitude and the time constant of persistence, mainly due to the additional capacitance induced by the large metallization and its impact on the passivation and the interface bulk/passivation.

4. CONCLUSION

With two detectors manufactured in the CEA LETI and Lynred clean rooms, seven technologies could be investigated through two characterization protocols. The classical technology with intermediate metallization and implantation size is investigated with detector MONO. We compare dark current and persistence response on larger and smaller values of these geometrical parameters with detector MULTI. The usual linear dark current shows minor differences both in absolute values and temperature dependency. At the nominal operating temperature of 100K great performances are met both on detector MONO and Met B technologies with dark current as low as $0.025e^-/s$. Generation current limits the dark current in the temperature range from 165K to 115K then a lower activation energy mechanism limits the dark current decrease on all the technologies probed. Technologies with the small metallization A have an initial negative non-linearity at temperatures below 115K that prevents to properly extract their dark current.

Persistence is characterized for the first time on detector from CEA and appears particularly relevant in a process line to probe faint effects with its non-uniformities and technological dependencies. Electrical stress protocol is easier to set up since capture/emission process from photo-generated carriers are not present. Its similarities with the DLTS technique can also be of great help to interpret the results of the electrical impulse response of the pixels. However the variable pixel

capacitance or conversion gain can mislead the interpretation. It minimizes the persistence response of technologies with large capacitance when plotted in volt unit and can induce too much uncertainties to convert the measured signal to equivalent charge in electrons unit.

Persistence amplitude is similar on detector MONO and technologies with large metallization size. The total amplitude on technologies with MET A is ambiguous due to the large capacitance variation with pixel voltage and fixed charges in the SCR. Implantation size has a minor impact but persistence still increases when this parameter increases, indicating the influence of traps in the SCR region. Time constants are not influenced by the implantation size, no different trap family is probed when the SCR size changes. However the non-linearity of the persistence is smoothed by the larger capacitance induced by the larger metallization size. Moreover the larger metallization may influence the surface of the pixel through the mechanical constrains and the electrical field applied on a larger region. These results point out the major issue of persistence, indicating that the linear dark current is a second order parameter, behind persistence and stability at low temperature.

A last remark concerns the differences between these detectors, that are test vehicles, and the detectors for the ALFA project. A good news is the large additional constant capacitance added on the pixel node for ALFA, whereas the node capacitance on our test detectors was intentionally very small compared to the diode capacitance [6]. Dedicated persistence characterization will be performed on ALFA detectors, we used here test components to set up the protocol and acquire knowhow on this particular phenomenon.

In future work we aim at comparing the persistence using both electrical and photonic stresses by mounting a cooled LED inside our cryostat. This additional test facility should bring even more information on the mechanisms involved in persistence and how to mitigate it directly from the process line.

REFERENCES

[1] M. W. Regan et L. E. Bergeron, « Zero dark current in H2RG detectors: it is all multiplexer glow », *J. Astron. Telesc. Instrum. Syst.*, vol. 6, nº 01, p. 1, févr. 2020, doi: 10.1117/1.JATIS.6.1.016001.

[2] B. A. McLeod et R. Smith, « Mitigation of H2RG persistence with image illumination », 2016, vol. 9915, doi: 10.1117/12.2233083.

[3] K. S. Long, S. M. Baggett, et J. W. MacKenty, « Persistence in the WFC3 IR Detector: an Improved Model Incorporating the Effects of Exposure Time », sept. 2015.

[4] S. Tulloch, E. George, et D. S. G. ESO, « Predictive model of persistence in H2RG detectors », *J. Astron. Telesc. Instrum. Syst.*, vol. 5, nº 3, 2019.

[5] O. Gravrand, L. Mollard, O. Boulade, V. Moreau, E. Sanson, et G. Destefanis, « Ultra low dark current CdHgTe FPAs in the SWIR range at CEA and Sofradir », 2011, vol. 8176.

[6] B. Fieque *et al.*, « Infrared ROIC for very low flux and very low noise applications », 2011, vol. 8176.

[7] R. M. Smith, M. Zavodny, G. Rahmer, et M. Bonati, « A theory for image persistence in HgCdTe photodiodes », 2008, vol. 7021, doi: 10.1117/12.789372.

[8] R. E. Anderson, M. Regan, J. Valenti, et E. Bergeron, « Understanding Persistence: A 3D Trap Map of an H2RG Imaging Sensor », *ArXiv E-Prints*, vol. 1402, p. arXiv:1402.4181, févr. 2014.

[9] A. Kobayashi, O. F. Sankey, et J. D. Dow, « Chemical trends for defect energy levels in Hg(1-x)CdxTe », *Phys. Rev. B*, vol. 25, nº 10, p. 6367-6379, 1982, doi: 10.1103/PhysRevB.25.6367.

[10] D. K. Schroder, *Semiconductor Material and Device Characterization: Third Edition*. 2005.

[11] S. Tulloch, « Persistence Characterisation of teledyne H2RG detectors », juill. 2018.

[12] T. Le Goff, N. Baier, O. Gravrand, J.A. Nicolas, T. Pichon, O. Boulade, « ROIC glow reduction in very low flux short wave infra-red focal plane arrays for astronomy », 2020, Paper No. 11454-118